Formation flying interferometry: from the coarse control to the science mode

Roland Frenkiel, Laurent Pirson, Jean-Baptiste Thévenet

Abstract

Interferometric missions with an instrument distributed on several vehicles in orbit allow deep space observations with an accuracy never reached, but demand a formation flying Guidance Navigation and Control (GNC) with a ultra-high level of precision. One ESA mission of that class, dedicated to exo-planets detection and characterization is nowadays identified: DARWIN. The different GNC stages, from the initial closed loop engagement at the end of deployment to the final control of the Optical Path Difference (OPD) and intensity mismatch used in science mode will be described.

First, a focus on the Navigation Process Unit (NPU) based on the Radio-Frequency (RF) sensor and the modes developed to achieve the coarse formation acquisition, the FDIR Collision Avoidance Mode (CAM) and the recovery after a failure will be given. The RF subsystem is developed by TAS under a CNES contract. Its aim is to provide a coarse relative position sensor and the Inter-Satellite Link (ISL), necessary for the finest mode. It covers a 30 km distance range, but will be adapted up to a 100 km range. It has 3 functional modes and is bi-frequency. The coarse mode covers all the directions of space and is based on the received powers measurements of several antennas scattered around each vehicle. The interferometric mode Before Ambiguity Raising (BIAR) measures the widelane phase shift and provides intermediate accuracy measurements in a privileged direction. The interferometric mode After Ambiguity Raising (AIAR) measures the carrier phase and provides 1 cm on inter-vehicles distance and 1 deg on Line of Sight accuracy measurements in the same direction, after a GNC maneuver. The two last modes require a triplet of antennas forming two orthogonal baselines. The CAM and the reconfiguration are based on the RF coarse mode. The CAM is used in a decentralized way to assure the robustness to formation level failures, whereas the reconfiguration is centralized in one vehicle to have a better coordination. The first control stage is based on the fine RF mode. These modes are generic to all formation flying missions.

Then, an overview of the EMMA configuration of DARWIN, a novel concept proposed by TAS, will be described from the system and GNC points of view. The Darwin GNC contains two more control stages in addition to the first one based on the RF sensor. The second stage based on

optical coarse and fine metrology and ionic or Field Electrical Emission Propulsion (FEEP) actuates the Collecting Spacecrafts (CS) relatively to the Beam Combiner Spacecraft (BCS) and acts on the formation's geometry. The third stage, internal to the BCS, acts directly on the scientific beam, adding an optical path with an Optical Delay Line (ODL) and changing its orientation with corrective tip/tilt mirrors based on piezo-actuators. The joint use of these two stages allows to meet the science requirements imposed on the OPD (<1nm) and the intensity mismatch.

Key words

Radio-Frequency Sensor; Collision Avoidance; Reconfiguration; Darwin Mission; Emma; Guidance Navigation Control.

1. RF Sensor Navigation Process Unit

1.1. RFS overview

The ``RF metrology and data-link'' subsystem provides both relative positioning service and inter-vehicle communication data link for high-altitude formation flying missions, where GNSS services are not available. The RFS is autonomous and may be used as is or at intermediate level to allow acquisition of ultimate precision optical sensor for instance

Today, a number of FF missions consider the RF instrument as baseline for “coarse positioning”. Optimal behaviour of the RF sensor is essential in this view.

Development activity is now going on through the FFIORD contribution of CNES to the Swedish PRISMA mission, for which several flight models of RFS are to be delivered by late 2008.

The RF subsystem is generic and multi-mission oriented (two to four vehicles, up to eight antennas per vehicle, configurable orbits...). It performs ranging and angular measurements on a large operational range (3 m to 30 km), based on GPS techniques. These measurements feed an embedded Navigation Processing Unit (NPU) which is interfaced with GNC and in charge of producing precise positioning data on a 1Hz-task basis: distance and Line of Sight (LoS), with 1 cm / 1° accuracy.

Secondary functionalities are provided by RFS:

- omni-directional coverage, providing safe conditions during deployment and failure recovery phases.
- S/C relative clock biases computation, since no on-board atomic clock is expected
- collision avoidance service

As for signal definition, the RF terminal transmits an S-band dual-frequency spread-spectrum signal to the other vehicles and receives the spread-spectrum signal transmitted by the other vehicles. Observing the received signal (code and carrier phase measurements) allows to retrieve distance and line of sight measurements. Furthermore, removal of clock bias (known better than 10 ns) implies the ability to exchange measurements between vehicles, and thus requires a data transmission channel. The latter Inter-Satellite Link (ISL) was indeed planned for positioning purposes, before being generalized to an OBC-OBC communication service. The currently available data rate of 12 kbit/s at 30 km will be further extended to 100 kbps for short inter-distances.

The carriers are modulated by both a PRN code to perform ranging measurements and the ISL data message, similarly to the GPS way.

Finally, access to antennas is performed via TDM: each Rx/Tx antenna is provided a 5 ms transmission sub-slot during which all remaining Rx/Tx antennas of the group operate in receiving mode.

1.2. Navigation performances

Two main modes are envisioned within NPU. The OBC user is responsible for mode switches using appropriate command to the RF terminal.

First, the deployment, re-configuration and collision avoidance tasks are achieved through the navigation coarse mode. It aims at providing omni-directional coverage and immediately-available distance and LoS estimates. Yet, accuracy is moderate (1 m for distance and 45 deg for LoS) but still reaches the requirement level for safely controlling the spacecraft formation. The coarse mode is actually based on pseudo-random code processing (measured between two Rx/Tx antennas) for

distance on one hand, and on RF power measurements for computing line of sight, on the other hand.

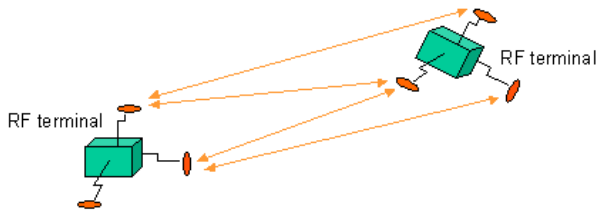

Figure 1-1:Coarse LoS from Power measurements

A noticeable feature here is that power measurements are actually managed by companion vehicle on a given Rx antenna within time sub-slots allocated to each transmitting antenna. Then

pieces of information are then broadcast back to host vehicle via ISL, which can further compare these measurement to evaluate coarse LoS.

Conversely, the acquisition of the final geometry is performed through the 3-antenna set, which uses an RF carrier interferometry technique for providing accurate knowledge of line of sight (better than 1 deg). As for distance, carrier measurements between Rx/Tx antennas lead to an accuracy below 1 cm. However, the so-called fine mode requires to precisely compensate measurement errors of various types (noise, electrical bias residual, multi-path) on the different signals, along with performing integer ambiguity removals (IAR).

Indeed, as stated above, desired accuracy in fine mode implies to make use of (non-ambiguous) carrier phase measurements. Since initially only code measurements are available as non-ambiguous distance estimates, they should serve as reference for carrier phase (CP) Integer Ambiguity Removal (IAR). However, they are far too biased for this purpose, which is the rationale for introducing the so-called widelane (WL) signal, obtained by combining both carrier phase measurements according to:

$$\varphi_{WL} = \varphi_1 - \varphi_2$$

Thus, a 3rd type of pseudo-range measurement with intermediate wavelength λWL is obtained, satisfying the following:

$$\lambda_{CODE} = 300m >> \lambda_{WL} = 1.7m >> \lambda_1 = 13cm$$

WL signal is non-ambiguous for LoS as long as the triplet baseline is lower than say $\lambda_{WL}/2 = 85\ cm$, which is not the case regarding distance. As a result, a succession of IAR processes (i.e. first on WL, then on CP) is achieved to eventually reach the desired accuracy on distance. Concerning LoS, a single step is required according to baseline length.

1.3. NPU Interfaces

In operating mode, relative positioning information (distance, LoS, and associated rates) is computed and precisely time-tagged by NPU (denoted by “snapshot processing” on Figure 7-1), from raw measurements provided by the digital section through RF terminal core software.

The NPU output feeds the position estimator in the GNC computer, while some low level aiding data is also provided to the terminal.

In particular, the NPU is in charge of computing clock relative de-synchronization between the spacecrafts. This allows to maintain TDMA frame synchronization within RF terminals for fast reacquisition purpose, in case of temporary signal loss. Similarly, time propagated pseudoranges and pseudorange rates are also provided to the RF terminal, along with Figures of Merit (FOM,

potential maximum errors), so as to provide Time/Doppler information and range scanning for reacquisition speed-up.

Besides, during nominal behaviour, NPU includes a module for selecting the best antenna couples between vehicles, based on power measurements transmitted through ISL. The receiving antenna within the RF terminal is chosen accordingly.

Conversely, outputs from the navigator are used by control loop obviously, but are also provided via appropriate command to the NPU for functional purposes:

- Cycle-slip detection and correction
- Direct GNC-aided IAR (see Section 1.1.3)
- Antenna wind-up detection and correction
- Power checking (coherence between estimated and measured received power)

1.4. From raw measurements to positioning

We describe hereafter the computations of distance and LoS in fine mode from raw measurements. Pseudoranges are equally denoted by "PR", with no reference to the considered signal, since the latter relates to the state of the algorithm in terms of IAR (see next section).

1.1.1. Distance computation

For the sake of simplicity, we consider only the basic case with two spacecrafts carrying a single Master (Rx/Tx) antenna, in order to explain the positioning principle:

- RF terminal i directly obtains two PR measurements:
  - $PR(T_{k/M},R_{i/M})$ from observing the signal transmitted by Master antenna of vehicle k and received by Master antenna of vehicle i.
  - $PR(T_{i/M}, R_{i/M})$ from observing the own transmitted signal of RF terminal i through its self-calibration loop (propagation delays inside both Tx and Rx sections of RF terminal i).
- Similar measurements $PR(T_{i/M},R_{k/M})$ and $PR(T_{k/M},R_{k/M})$ from RF terminal k are transmitted to RF terminal i via ISL as shown on Figure 1-2:

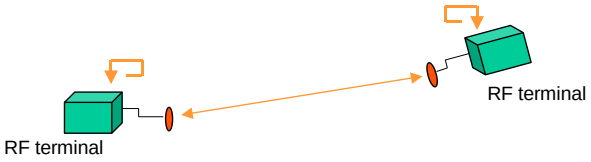

Figure 1-2: Distance processing scheme

Processing of distance and relative clock offset are then obtained by the NPU unit according to:

$$D = \frac{PR(T_{k/M}, R_{i/M}) + PR(T_{i/M}, R_{k/M})}{2} - \frac{PR(T_{k/M}, R_{k/M}) + PR(T_{i/M}, R_{i/M})}{2} \qquad \tau_{ki} = \frac{PR(T_{k/M}, R_{i/M}) - PR(T_{i/M}, R_{k/M})}{2} - \frac{PR(T_{k/M}, R_{k/M}) - PR(T_{i/M}, R_{i/M})}{2}$$

However, it should be kept in mind that filtering is necessary, and so are additional corrections to account for miscellaneous measurement errors, among which:

- electrical bias inside front-end, antenna center of phase position error,
- multi-path error (corrections available in tables addressed via LoS value and obtained from test campaigns in anechoid chamber)

These corrections are applied by NPU from embedded parameter tables. One table is provided for each antenna and may be updated (uploaded) during flight operations.

In addition, since measurements are not performed at a common time within the formation, due to clock de-synchronization, the Navigation Process Unit is able to store measurements, perform samples selection and propagate companion measurements using Carrier phase Doppler information so as to re-synchronize measurements to a common time, up to first order.

This functionality is essential to account for maneuvers and S/C relative dynamics, in order to reach the specified accuracy regarding distance and clock offset computations. This task is obviously performed before combining measurements as described in the equations above.

1.1.2. Fine LoS computation

Similarly, we consider for simplicity a single triplet, (i.e. one Master and two Slave (Rx-only) antennas), in the formation, as shown on Figure 1-3.

1. RF terminal i directly obtains directly obtains five PR measurements:

- $PR(T_{k/M},R_{i/M})$ from observing the signal transmitted by Master antenna of vehicle k and received by Master antenna of vehicle i.
- $PR(T_{k/M}, R_{i/Sx})$ and $PR(T_{k/M}, R_{i/Sy})$ from observing the signal transmitted by Master antenna of vehicle k and received by Slave antennas X and Y of vehicle i.
- $PR(T_{i/M}, R_{i/M})$, $PR(T_{i/M}, R_{i/S})$ own transmitted signal of RF terminal i through its self-calibration loop (propagation delays inside both Tx and Rx sections of RF terminal i).

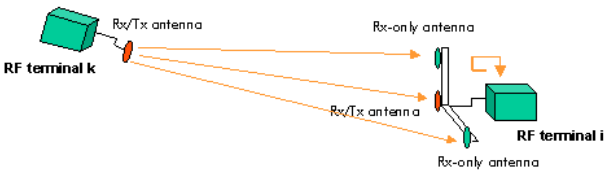

Figure 1-3: Fine LoS processing scheme

Processing of fine LoS components is thus obtained as:

$$X_{LoS} = \frac{PR(T_{k/M}, R_{i/M}) - PR(T_{k/M}, R_{i/Sx})}{L_X} - \frac{PR(T_{i/M}, R_{i/M}) - PR(T_{i/M}, R_{i/S})}{L_X},$$
$$Y_{LoS} = \frac{PR(T_{k/M}, R_{i/M}) - PR(T_{k/M}, R_{i/Sy})}{L_Y} - \frac{PR(T_{i/M}, R_{i/M}) - PR(T_{i/M}, R_{i/S})}{L_Y}$$

where Lx and Ly stand for baseline lengths.

Finally, note that LoS and distance rates, as well as clock drifts, are obtained by the variation of the previous quantities between two subsequent 1hz steps. In this case, only carrier phase raw measurements are involved in the computations since carrier phase variation is non ambiguous at the first place.

These computations are used among other things to compute an estimated time of collision between vehicles. Consequently, a warning is delivered to the user when the corresponding value reaches some given threshold.

1.5. IAR algorithms

Three different methods for ambiguity removal are forecast, depending on the configuration and the multipath environment.

1.1.1. Filtered IAR

This type of IAR is used when multi-path error is low (or well-mitigated) and no valid direct-aiding data is available from GNC. In this case, successive smoothing of code (and WL measurements if necessary) are performed with the carrier phase measurements, respectively. For each process, the filtered signal is compared to the ambiguous one to retrieve the value of ambiguity via a nearest integer rounding operation as depicted on *Figure 7-2*. Once the CP ambiguity is eventually known, the measurement value is propagated to current time thanks to integrated Doppler measurement.

Note that in the generic case the process may be equally run for distance or LoS. However, since the baselines (distances between master and slave antennas) foreseen on most missions are small enough (see 1.2), LoS from WL is non-ambiguous from the start.

As a result, the method involving 2 subsequent IAR steps will be usually necessary for distance only.

1.1.2. GNC-aided (LoS only) IAR

The context here corresponds to poor multi-path corrections and no valid direct-aiding data available, so that both other proposed IAR methods do not apply. The following alternative is proposed: spacecrafts are first approximately aligned (via knowledge of LoS valid from WL). Then

a rotation of host vehicle is achieved around boresight axis, with precise knowledge of the rotation angle (provided by Star Tracker). It can then be shown that measuring and filtering F1 path difference variation during the rotation allows to safely remove the ambiguity on F1 via an additional nearest integer rounding operation, even in large MP environment.

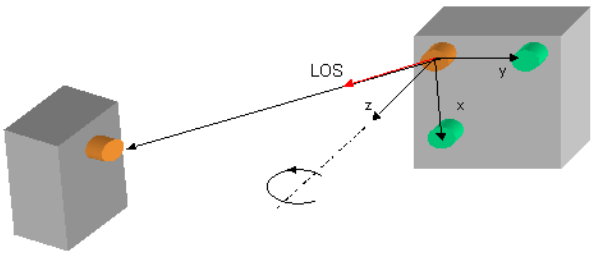

Figure 1-4 : GNC-aided LoS IAR

1.1.3. GNC direct-aided IAR

When (recent) valid direct-aiding data is available from GNC, direct-aided IAR is achieved. This typically concerns steady state of the on-board navigator, when a momentarily loss of signal occurs, due for example to an antenna handover. The Navigation Processing Unit is provided with time-tagged non-ambiguous data and associated FOM. NPU then propagates these data to current time and re-computes current ambiguity by combining ambiguous measurements with aiding data, in accordance with FOM.

1.6. From coarse mode to ultimate accuracy

The nominal sequence of IAR after acquisition is finally depicted on Figure 7-3.

2. Collision Avoidance Mode (CAM)

Because the measurements must be available in all the directions, the CAM will use the coarse mode of the RF. The collision avoidance consists on re-directing one or several flyers from some directions to avoid. The low precision of this mode is then not constraining for the CAM.

2.1. Hypotheses on the collision risks

The collision risk has been treated in the case of missions at the Lagrange points, where the gravity gradient is negligible. Three cases of failure have been identified as leading to a collision risk: a thrusters leak, an on-board computer failure or a guidance error. A fourth identified case is the kinematical conditions after the launcher exit. But knowing the values of the relative velocities after the launcher separation if no other strategy than the closed loop inter-S/C distance control is used, this technique cannot be applied. For that particular problem a strategy of separation based on initial velocities with respect to the launcher is envisaged.

During a thrusters leak, the S/C can accelerate or maintain its velocity thanks to the other thrusters, but cannot decelerate. Finally, the maximum relative velocity with respect to another S/C is given by the nominal guidance profile during a manoeuvre.

A computer failure leads first to the reboot which needs 30 s and in the worst case to the cold start of the RF sensor, which needs 5 mn to give a full position determination capability. Then, the kinematical conditions are similar to the thrusters leak case.

The guidance contains mechanisms able to detect some errors. Then, this kind of error will not create the worst dynamic conditions.

Finally, the case of a thrusters leak is retained and a maximum relative velocity is chosen such that the ratio distance/maximum velocity remains higher than a reasonable time, as depicted in *Figure 7-4*.

The maximum relative velocity is then a function of the initial and final inter-S/C distance. A value of some cm/s is chosen as an illustrative case.

2.2. FDIR CAM engagement and CAM disengagement

The transition from a nominal mode (first stage based on the RF sensor for example) to the CAM is decided by the calculation of a FDIR collision flag in each S/C in good health with respect to all the others. This one is based on the measurement of the relative position by the RF and on an estimation of the relative velocity. The axial component of the relative velocity is measured by the RF whereas the ortho-axial ones are derived from the relative position.

A threshold on the distance dmin (8m for example) and a threshold on the time to reach this distance in the future (some hundreds seconds for example) are defined. The collision of flyer F1 with flyer F2 is anticipated when the linear extrapolation of F1's trajectory over the time threshold intersects with the sphere of radius dmin centred on F2. Hence, a collision probability is calculated as described in [1].

A collision risk flag could be raised if this collision probability is over a threshold, but this flag would have the drawback to switch several times due to the spatial and time varying errors on the different estimated parameters. This means the FDIR would engage the CAM, disengage it and could possibly re-engage it on a time period of some hundred seconds. This case is illustrated in Figure 7-5: using a common snapshot indicator to transit from a nominal mode to CAM and from CAM to a nominal mode is not a good strategy. Then, it is proposed to calculate these 2 transitions in a slight different way.

The transition decision from nominal mode to CAM is important and should be taken only when the collision risk is assessed with no false alarm. To raise the FDIR flag only in the accurate

case and stop the CAM only when the collision risk is negligible, this one is evaluated in over a gliding period and a hysteresis trigger is used: the collision probability Pc1 is calculated only with current informations (except of course the way to estimate the relatives positions and velocities which are outputs of low-pass filters). Two intermediary probabilities are then introduced. The first one Pc2 is the average of Pc1 on the last T2 seconds. The second one Pc3 is the average of Pc1 on the last T3 seconds. The FDIR flag is set to true if Pc2 increases above a threshold thr_Pc2 and to false if Pc3 decreases under another threshold thr_Pc3, as described in Figure 2-1.

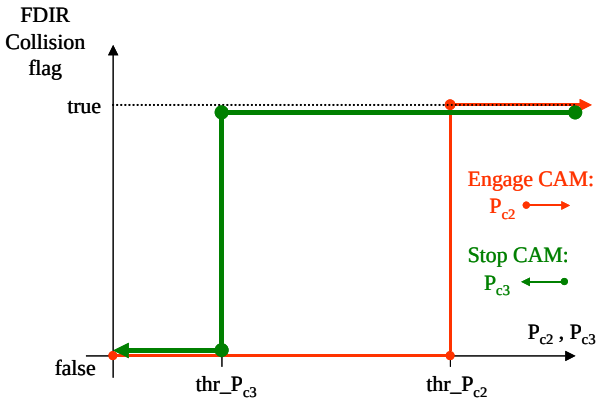

Figure 2-1: FDIR engagement and disengagement logic - P_{c2} = average of snapshot estimated collision probability P_{c1} on last T_2 s - P_{c3} = average of P_{c1} on last T_3 s

This technique allows to have only one transition to CAM to achieve the safety of the formation, which is an absolute necessity knowing the chronologic constraints induced by the command/control subsystem.

2.3. CAM Algorithm

The Collision Avoidance Mode algorithm is very simple. In each flyer in good health called F2 a collision avoidance force is calculated. This force is the sum of one term deriving from a potential given in Équation 1 and other terms respectively orthogonal to the Line of Sights of each of the other flyers, including the failing one. Knowing that only the case of single failure is treated, only one component orthogonal to the Line of Sight should be non null. However, the case where F2 flees F1 and then artificially creates a collision risk with F3 is implicitly treated and the algorithm is able to re-optimize the escape direction.

The potential is expressed in the considered flyer's reference frame. It gets very high when another flyer is close to F2 (and also very distant for scattering avoidance). The potential in the flyer i depends only on the inter-flyers distances. It can be plotted in 2 dimensions (as seen on Figure 2-2) and is expressed the following way:

n_sat Number of flyers in the formation

$Xm_{j/i}$ Measurement of the relative position of flyer j by the flyer i in its frame

$$V\left(\left(Xm_{j/i}\right)_{\substack{1\le j\le nsat\\ j\neq i}}\right)=\sum_{\substack{1\le j\le n\_sat\\ j\neq i}} f\left(\left\|Xm_{j/i}\right\|\right)$$

$$f(d)=\alpha_{\text{anticoll}}\cdot\left(d_{\min}-\min\left(d,d_{\min}\right)\right)^2+\beta_{\text{anticoll}}\cdot\left(d_{\max}-\max\left(d,d_{\max}\right)\right)^2$$

Équation 1: Expression of the CAM potential

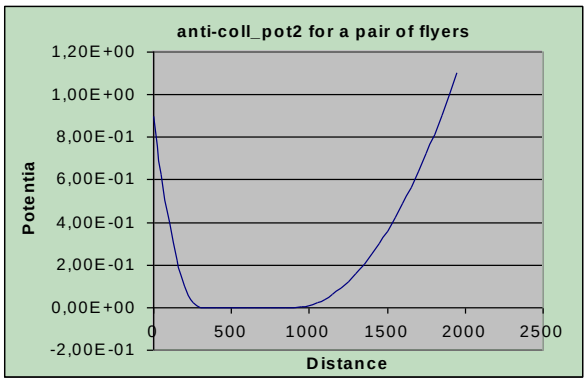

Figure 2-2: Collision avoidance potential for one pair of flyers.

First, the snapshot collision indicator proper to each other flyer F1 is calculated the same way as the one for the elaboration of the FDIR transition flag, but with lower thresholds, as this mechanism does not raise any alarm. If this flag is false, the orthogonal force is null. If this flag is true, an escape direction orthogonal to F2's Line of Sight and avoiding the other flyers is determined. The norm of the escape force is a constant fixed at a value lower than the thrusters force capacity, such that the complementary force budget is allocated to the term deriving from the potential.

2.4. Simulation of engagement and execution of CAM

A simulator of the collision avoidance mechanism has been realized. The first scenario is the following:

- There are 2 flyers in the formation

- Flyer F1 is at 30m of F2 and its velocity (0.02 m/s) is directed toward F2

- The formation is initially in Stand-By Mode (SBM): there is no position control on any flyer thanks to a FDIR mechanism other than the collision avoidance surveillance.

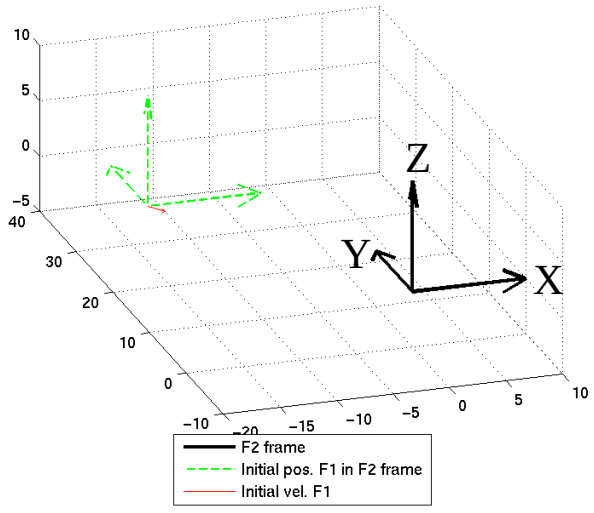

Figure 2-3: CAM - Initial conditions

On Figure 7-6, it is visible that the collision risk is not initially identified because the different filters used to estimate the relative positions and velocities are bad initialized (the angle between the opposite of the LoS of F1 and its relative velocity is estimated at 60 deg whereas it is 0 deg). After a convergence time corresponding to the time constants of theses filters, the collision probability has a high value and the CAM is engaged (Figure 7-7). The collision avoidance is executed correctly as seen on the trajectories (Figure 7-9) and on the inter-flyer distance profile (Figure 7-10).

3. Overview of the Emma GNC

3.1. The Emma Arrangement

The proposed Emma configuration is a new out-of-the plane arrangement. It features three collector spacecrafts (CS) and one beam-combining spacecraft, with telescopes focusing the beams on a Beam Combiner Spacecraft (BCS) (cf. Figure 3-1 and Figure 3-3). This arrangement allows both to maximise science return, and to dramatically alleviate engineering constraints thanks to a fully non deployable concept, significantly enhancing the system reliability.

Emma Triangular Orthogonal Three-Telescope Nuller (TO-TTN) configuration (with a ratio of 1 between orthogonal sides) features 3 Collector Spacecraft (CS) and one BCS. The CS are located on a plane perpendicular to a virtual paraboloid focused on the BCS, which summit is at around 1200 m of it. Their distance varies between around 20 and 170 m, according to mission needs translated into different baselines, as seen depicted on Figure 3-3.

Following this mission study, an alternative to TO-TTN has been studied on in-house funding by Thales Alenia Space, based on future Ariane 5 improvements which could afford a higher launched mass and hence allow the accommodation of a fourth CS (with a diameter smaller that the one issued in TO-TTN configuration). This X-Array configuration (cf Figure 3-2) presents some advantages w.r.t. TO-TTN in terms of symmetrical optical path and alleviation of constraints due to Variability Noise. The system architecture of EMMA is presented in [2].

Emma features a specific metrology subsystem involving a three-stage set of RF and optical sensors, coping with formation flying requirements and ensuring a challengingly low level of OPD in terms of value and stability, constrained by Variability Noise which imposes to implement an internal metrology stage after the first three correction stages.

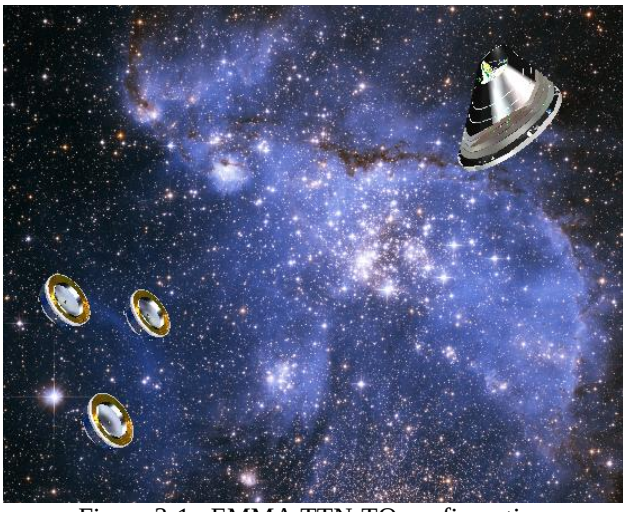

Figure 3-1 : EMMA TTN-TO configuration

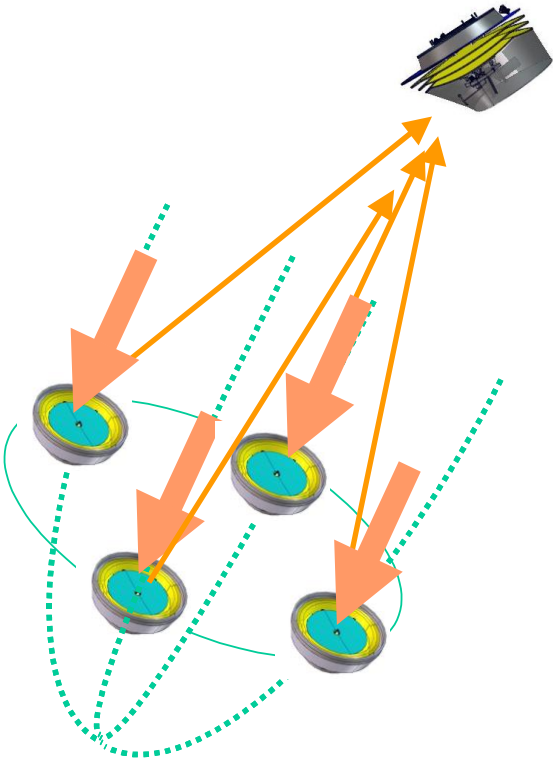

Figure 3-2 : EMMA X-Array configuration

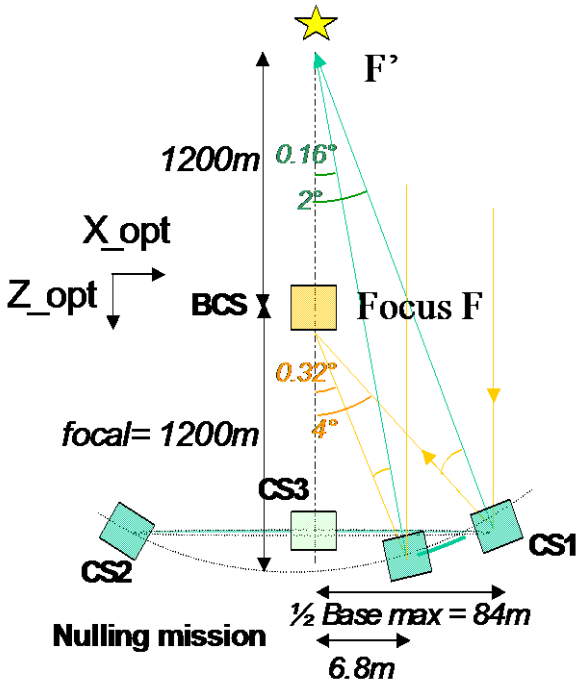

Figure 3-3: Geometry of the TTN-TO EMMA configuration

3.2. GNC Requirements

DOF	Requirements	Control level stage
δ_X	Fixed by ODL stroke while < 1cm	2nd
δ_Y	Fixed by ODL stroke while < 1cm	2nd
δ_Z	Fixed by ODL stroke while < 1cm	2nd
θ^{CS}_X	0.7as	2nd
θ^{CS}_Y	0.7as	2nd
θ^{CS}_Z	2as	2nd
θ^{BCS}_X	0.7as	2nd
θ^{BCS}_Y	0.7as	2nd
θ^{BCS}_Z	<1arcmin	2nd
CS/SMW tip/tilt	73mas	3rd
Inter CS tip/tilt	25mas	3rd
OPD	0.1nm (TBC)	3rd

Table 3-1: GNC requirements

In Table 3-1, dX, dY, dZ represent the acceptable errors on the CS relative positions with respect to the BCS. The requirements on attitude for the second control stage concern only the inertial one: each S/C is able to control independently its own inertial attitude thanks to a very accurate STR. The relative orientation of the scientific beam coming from the CS with respect to the recombination fibre (SMW) is only dealt with by the third control stage level in the BCS. The control stage levels are defined in detail in §3.3, §3.4 and §3.5.

Note that the first external control stage is only used to ensure the deployment of the formation and the acquisition of the second external control stage and thus does not appear in the table above.

The axes used are the BCS Optical Reference Frame (Xopt, Yopt, Zopt), inertial frame with Zopt in the anti-direction of the observed star.

The conclusions of the study are the following:

- The main drivers are the stroke of the actuators of the third control stage, meaning ODL and tip/tilt mirrors,
- The oversizing of the primary mirror diameter can become a constraining parameter if the lateral drift of the CS w.r.t. their target position becomes too important, as a matter of fact in such a case there is some loss of flux and the equality of intensity between the different beams can no more be achieved.
- The optical aspects have not been judged constraining (w.r.t. the others ones).

In addition to these requirements, the typical sequence that must be achieved for each target star is composed of :

- 3 baselines to consider: resizing between each baseline are discrete manoeuvres during which observation is interrupted (only interference fringes must be kept)
- for each base: 180° continuous rotation around star direction (the paraboloid axis) while observations are realised and thus final requirements on OPD and tip/tilt maintained,
- At the end, slew of the formation towards a new target star without keeping the fine formation topology.

3.3. First control Stage

The first stage is based on RF sensors, its objective is to realize all the coarse formation flying control and to reduce the errors in order to acquire the second stage. This stage is common to all the closed loop tight formation flying missions.

The accommodation of the RF antennas offers for each S/C a 4π-steradians coverage :

- An antenna triplet is accommodated on each CS, this triplet is used for the fine mode when the formation configuration is nominal: the triplet is accommodated on the side of the CS, between the warmest V-Groove. Thus the normal of the triplet plane is nearly pointed towards the BCS . The lever arm between the three antennas can be relatively important: this is an advantage since the LOS error is directly inversely proportional to the lever arm between the antennas. Three additional Rx/Tx antennas are located on the CS lateral faces to ensure the 4π steradian coverage, they are used in coarse mode,

- On the BCS, 4 Rx/Tx antennas are accommodated to cover the whole space and ensure that in nominal configuration at least one antenna is seen by the triplet of each CS.

The actuation of the first external control stage is realized thanks to milli-Newton ionic propulsion, preferred to cold gas mainly for mass consideration. The ionic propulsion system must allow a 6 DOF control capacity for each S/C. This is achieved thanks to a 12-thrusters configuration, in addition to it, 6 thrusters are foreseen for redundancy consideration.

A first step is the rough configuration of the formation in a centralized way with the RF coarse mode. Then, the GNC switches to a decentralized control to make the IAR and then switches to the second control stage. This strategy has the advantage to take into account the fact that the trajectories should not cross each other at the same date (nominal collision avoidance). To spotlight the interest, a simulation consisting of exchanging 2 CS relative positions with respect to the BCS has been run (Figure 7-11 and Figure 7-12). The control law contains a bypass in case the distance between 2 satellites get too small. The thresholds are tuned such that the bypass is achieved without risking to raise the FDIR collision flag.

After the rough configuration, the control of each CS w.r.t. the BCS can be done autonomously since the RF measurements are directly available on each CS. Taking into account this consideration, each CS can reach independently in a decentralized way its nominal position w.r.t. the BCS using, as soon as possible (ie BCS in visibility of the CS antenna triplet) the RF BIAR mode. Then it realizes the Integer Ambiguity Resolution manoeuvre to acquire the RF AIAR mode and improves the position control in order to acquire the sensor of the second external control stage.

3.4. Second External Stage

The second stage is based on optical sensors. The objective of this external control stage is to improve the accuracy of the formation in order to be compatible with:

- no loss of intensity in the transmission of scientific beam from CS to BCS (thanks to sufficiently accurate pointing and relative positioning),
- the acquisition conditions of the Fringe Sensor,
- the stroke of the ODL and tip/tilt mirror,
- a residual OPD and tip/tilt error compatible with the 3rd stage high-frequency filtering capability.

The 2nd stage uses specific optical position sensors:

The ULLIS sensor is a lateral (with a few 10µm accuracy at 1200m) & longitudinal (with an accuracy <3mm at 1200m) relative position sensor, based on a divergent laser and a corner cube network. One of the primordial advantage of this sensor compared to a collimated sensor is that its

divergent cone is compliant even at a distance of 1200m with the 1° RF accuracy and also with the variation of target BCS-CS relative attitude due to the baseline changes (±2°) (cf. Figure 7-13); moreover its accuracy allows a formation control compatible with fringe acquisition It has been breadboarded by Thales Alenia Space as described in [3].

Our baseline accommodation solution is today three ULLIS sensors on BCS using scan tip/tilt mirrors (the ones used for the science beams reconfiguration) to ensure the correct pointing towards the CS. Retroreflectors are located around the CS mirrors, thus the inter-retroreflectors distance (2a) is quite important (>3m) which is advantageous for the accuracy.

The second optical sensor is the Fine Relative Longitudinal Sensor (FRLS) based on interferometer concept using collimated laser: this sensor allows to improve the coarse ULLIS longitudinal measurement accuracy by measuring distance with a few nm accuracy.

These sensors have to deal with the dynamics and the variable geometry of the TO-TTN Emma arrangement.

A High Accuracy STR mounted on the optical bench of each satellite will be used for accurate measurement of inertial attitude. This sensor will take the relay from the first control stage STR. Its Field of View will be reduced to a few degrees.

The actuation of the second control stage will be realized by the ion milli-Newton propulsion for the coarse convergence phase, the slew and resizing maneuvers and by micro-Newton FEEP thrusters for the control during observation (low thrust with low level of noise). As for the milli-propulsion, a 6 DOF capacity is required on both CS and BCS. Considering the mechanical and thermal constraints, a nominal accommodation based on 12 thrusters is proposed, 6 are added to ensure a complete redundancy.

The control strategy used with the second stage is first to control each CS w.r.t. BCS thanks to the ULLIS measurement. The control of each BCS-CS arm can be done independently, the control is partially centralized since the measurements are available on the BCS and the movement is realized by the CS. The guidance is directly imposed by the scan tip/tilt mirror located in the BCS optical bench and through which the ULLIS laser passes. Thus from the ULLIS point of view the target is always at the centre of the detector allowing to remove coupling between lateral and longitudinal error measurement.

Then, the additional FRLS are used during the observation: the second control stage loop is kept closed during the observation in parallel to the third one. The CS are controlled permanently and they cannot drift from their target positions. Thus the ODL has not to be unloaded (once the fringes have been found, the ODL works around an equilibrium position and does not have to compensate any CS external drift) and the mission's Duty Cycle is not affected. On the other hand, a

continuous control with the second stage implies that the metrology noise shall be very low, otherwise its contribution to OPD will make impossible the OPD control under the requirement of less than 1nm. The ULLIS optical sensor is not compatible with such a strategy, notably due to the coupling between its lateral position error measurement and the BCS attitude, which, due to the long lever arm has a huge impact on CS position control performances. We propose then to use a Fine Relative Longitudinal Sensor (FRLS) to control the CS drift during the observation. The goal of this sensor is not to measure the distances between S/C but only their distance variations. In this functional mode, its noise is no more than a few nm. The drawback is the need of a steerable mechanism since this sensor uses a collimated beam and the formation geometry varies with the baseline, as can be seen on Figure 3-3: due to the mirror effect, the CS point toward the point F' on the Virtual Paraboloid axis, distant of 2 focal lengths from its summit, whereas the FRLS beam points toward the BCS at its focus F. The angle between these 2 directions varies with the baseline from 0.16° to 2°.

For the 2nd stage; six FRLS will be accommodated (2 per CS) in order to measure the 6 sides of the tetrahedron. In the case of the X-Array configuration, the formation is a pentahedron on which a minimum of 9 sides have to be measured. Then a centralized estimator has been developed. Its objective is to collect in the BCS all the sensors measurements available in order to obtain an accurate estimation of the relative positions of the CS, in order to limit as much as possible the residual OPD error after the second control stage (at least at a level compatible with the capability of the third control stage to finally ensure an OPD better than the requirement). The inputs of this estimator will be the 3 ULLIS lateral measurements, the 6 inter-SC distances measured by the FRLS and the positions of the 3 ODL (which give an information about the OPD after the second control stage). One of the main features of this estimator is that it delivers an estimation of the relative positions of each CS w.r.t. BCS in a spherical inertial frame (relative position given by triplet (φ, ψ, d)) allowing a control in that frame. This is very interesting to limit the residual noise transmitted on the OPD. The control will be done in a centralized way and the output of the estimator will allow to compute commands at BCS level for each CS: these commands will be sent to each CS for execution via the ISL.

With such an estimator, the residual OPD rate after 2nd stage could be reduced to a few nm.s-1. This control performance becomes compatible with the OPD requirements and an ODL driving frequency equal to the Fringe Sensors sampling frequency.

3.5. Third Control Stage

Lastly, the third stage allows to reach the final performance on OPD and tip/tilt. It is located in the BCS optical bench and acts directly on the scientific beam thanks to optical actuators (ODL and tip/tilt mirror) to correct the residual errors of the second stage measured on OPD and tip/tilt. The measurements are delivered by a Fringe Sensor (FS), concept DWARF developed by ONERA. Figure 3-4 gives a schematic view of the third control stage.

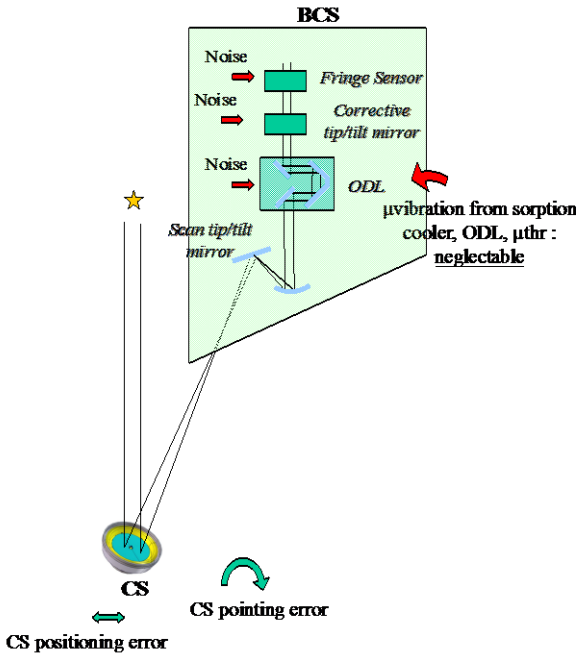

Figure 3-4: Third control stage based on ODL and corrective tip/tilt mirror

The 3rd stage controller of the OPD has then been designed in order to reach the OPD requirement. The OPD control loop is symbolized on the *Figure 3-5*:

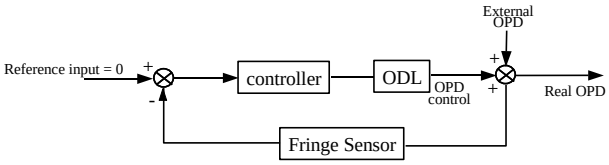

Figure 3-5: OPD control loop

The external OPD is seen as a disturbance with low frequency components (<0.1rd/s) and amplitude depending on the performance of the 2nd control stage. The goal is to reject these low frequencies as much as necessary to reach the OPD requirements. We thus considered the closed-loop transfer function between external OPD and the real OPD:

$$\frac{\text{Real OPD}}{\text{External OPD}}(s) = \frac{1}{1 + \text{controller}(s) \times \text{ODL}(s)}$$

The asymptotic behaviour of this transfer function is visible on Figure 3-6 and Figure 3-8:

- For High frequency: equivalent to 1,
- For low frequency: equivalent to $\frac{1}{controller * ODL}$

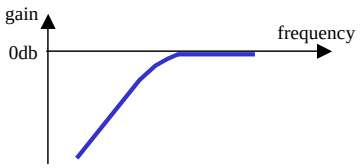

Figure 3-6: Asymptotic behavior of the transfer function between external OPD and OPD real

The high attenuation in the disturbance frequency range (<0.1rd/s) is brought by:

- "integrator" type controller (number of integrators function of the required attenuation level)
- a "high frequency" control bandwidth: this lets few possibilities to add a high frequency filtering in the controller, thus there is no additional low-pass filter on the external OPD output by the 2nd stage. Hence, it is important to have a performing controller at the 2nd stage level in order to reduce as much as possible the residual (external) OPD rate and to filter the high frequencies coming from the second stage.

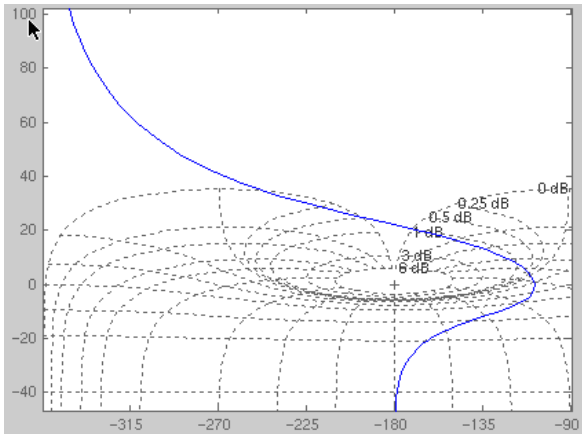

Figure 3-7: 3rd stage - controlled open loop transfer function - stability margins : Gain >20dB, Phase >60°

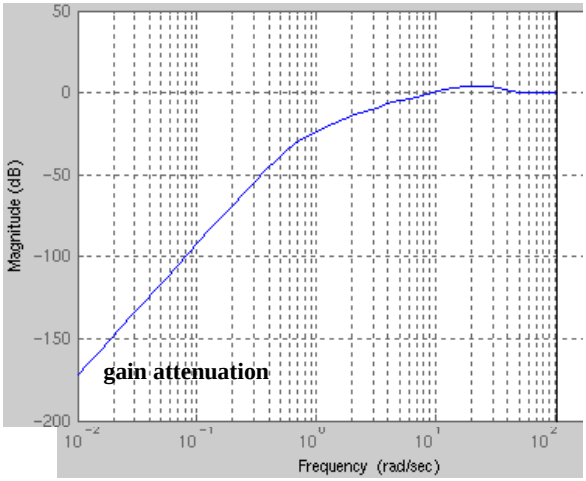

Figure 3-8: 3rd stage - Closed-loop transfer function between disturbance (external OPD) and real OPD : attenuation better than 100dB below 0.1rad/s

4. Conclusions

Different activities in TAS have allowed to design all the stages of an interferometry mission, from the initial configuration to the science mode, and recommend the technological developments on the road toward DARWIN, among which DARWIN System Assessment Study ESA contract, in-house funded Research and Development, and Formation flying RF metrology development in the frame of the FFIORD (Formation Flying In Orbit Ranging Demonstration) contribution of CNES to PRISMA mission.

The RF subsystem is necessary and designed to fit to all the formation flying missions. It will be used for the coarse 1st control stage, or equivalent in other missions than Darwin, but will remain activated in open loop during all the mission for the FDIR surveillance and the collision avoidance.

The design of the Emma control is a first iteration which has proved the feasibility of the GNC, while maximising the science return of the Darwin mission. This has been achieved through the definition of the accurate set of sensors and actuators and their required performances, in accordance with a realistic technological roadmap.

5. Following Activities

The baseline of the GNC for Emma has been designed. The next envisaged step is divided into 3 orientations:

- Optimize the performance of the science mode using advanced control techniques: considering the 2^{nd} and the 3^{rd} stage together and the coupling translation/rotation, design a multi-variable control law. A possible decentralised command, each CS using a part of the measurements is envisaged, assuming the global optimality of the formation. The extension of the estimation of the geometry in the case of a formation with 5 S/C (typically the Emma X-Array) will be done.
- Optimize the thrusters consumption and the maneuvering time during the initial configuration or reconfiguration.
- Reflection about the calibration issues which will be an important point on the DARWIN (or any other interferometric) mission.

6. Acknowledgements

The authors would like to thank Philippe Gondoin (Technical Responsible of the Darwin System Assessment Study), Roland den Hartog (in charge of Darwin performance) and Finn Ankersen (in charge of Darwin GNC), as well as past and present ESA members involved in Darwin studies and developments.

Many people were involved in the Darwin System Assessment Study, inside Thales Alenia Space or inside our industrial team. Thanks for their contribution and assistance.

References

1. Frenkiel R., et al., Radio-Frequency Technology and GNC (Guidance Navigation and Control) for Formation Flying, 57th IAC, 2008, Valencia
2. Sghedoni M., et al., Novel Emma Arrangement for DARWIN Mission, ESA 3rd International Symposium on Formation Flying, Mission and Technologies, 2008, Noordwijk
3. Napierala, B., et al., ULLIS - A Combined Optical Metrology Sensor with Minimum Accommodations Constraints, ESA 3rd International Symposium on Formation Flying, Mission and Technologies, 2008, Noordwijk

7. Annex: Figures

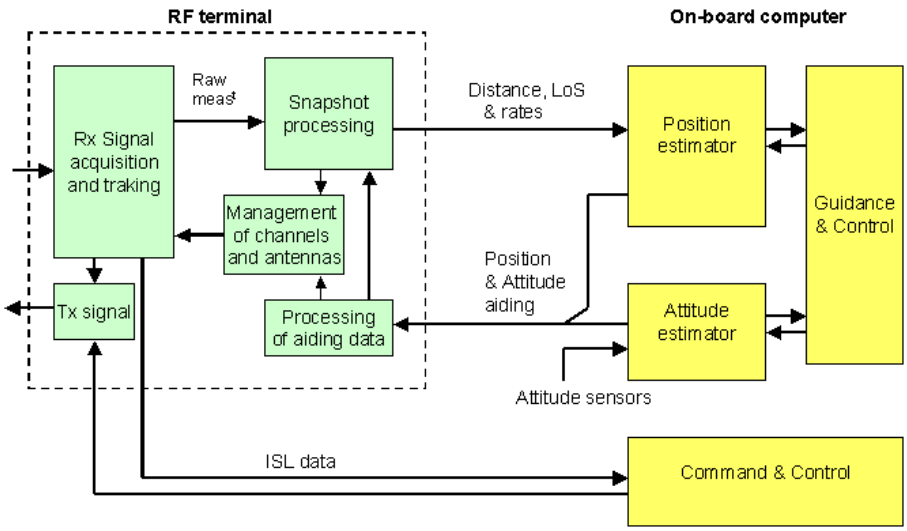

Figure 7-1: Interface with On-Board Computer

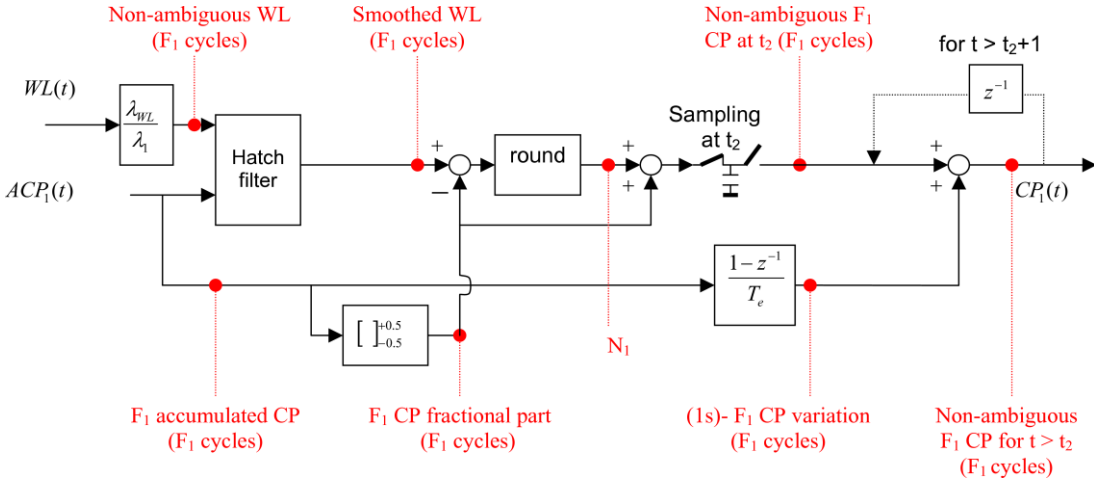

Figure 7-2: Filtered IAR

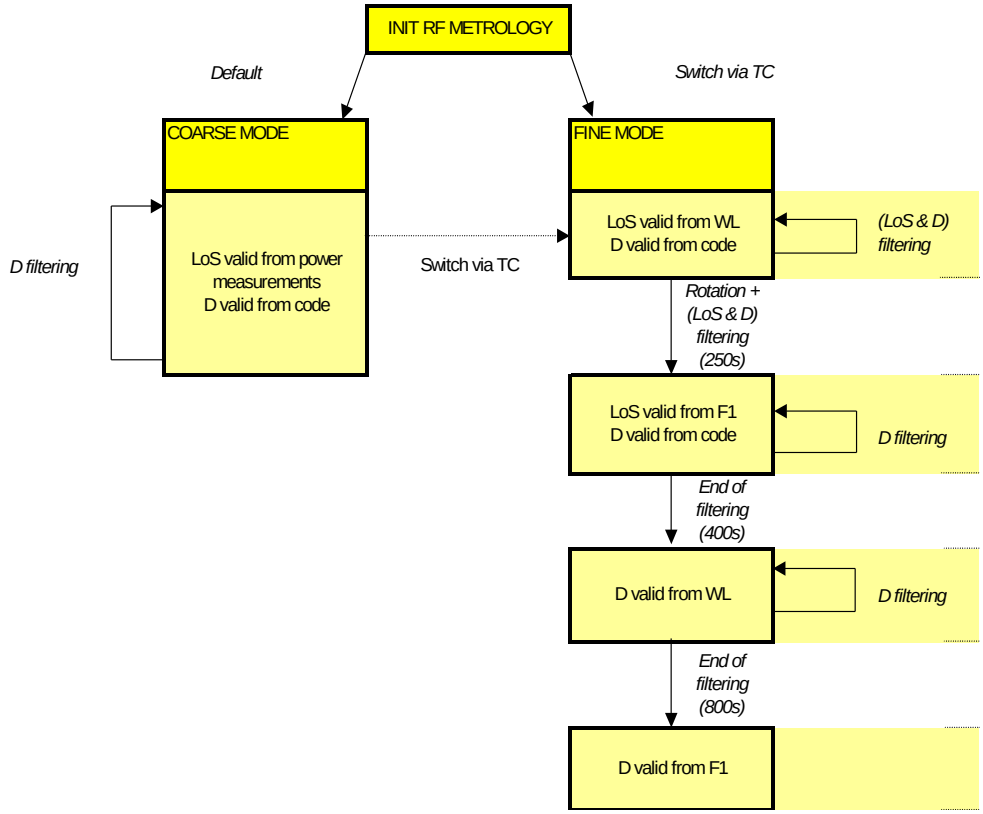

Figure 7-3: IAR sequence

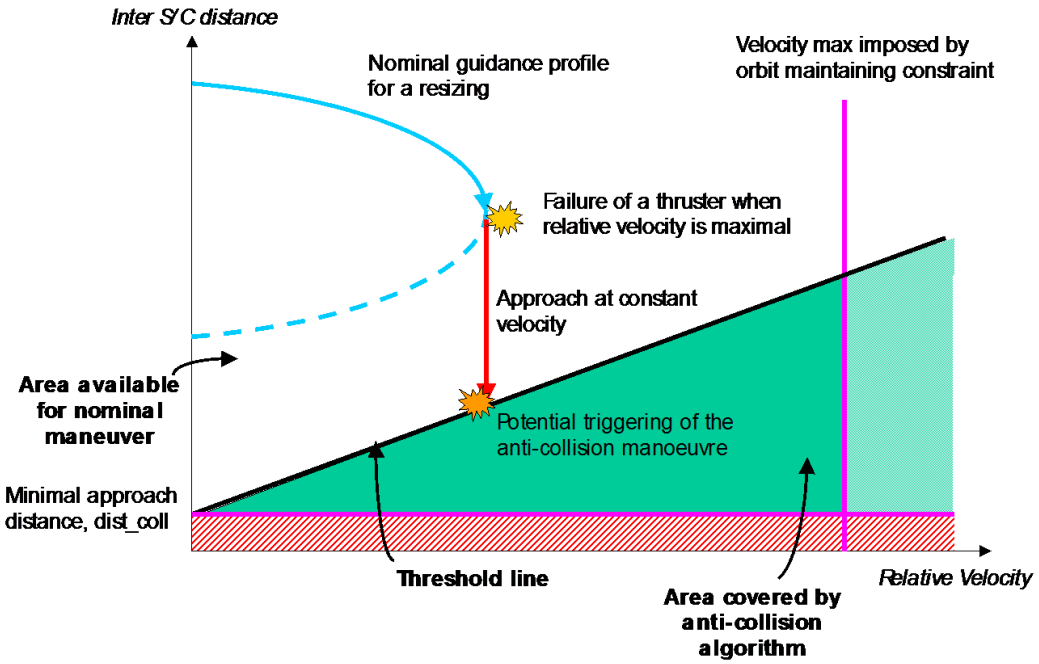

Figure 7-4: Diagram relative velocity / inter-S/C distance for guidance profile

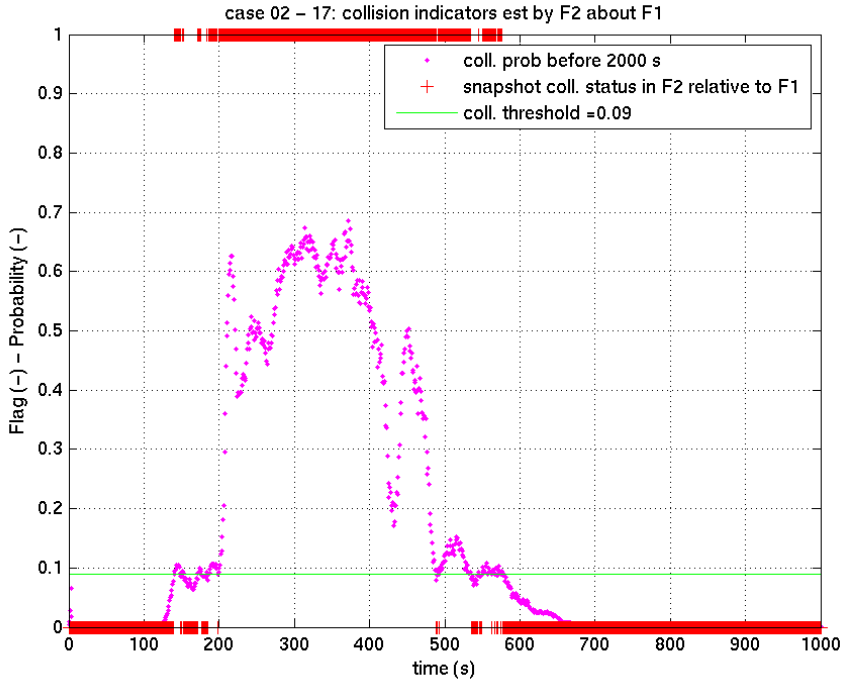

Figure 7-5: Example of snapshot collision status calculated in F2 relative to failing F1: in this simulation, the collision status is true when the collision probability is > 0.09 - The numerous transitions of this status (false⇒true⇒false⇒true⇒false⇒true⇒false...) are not suitable for a FDIR transition and proves the need to calculate a flag with only 2 transitions (false⇒true⇒false)

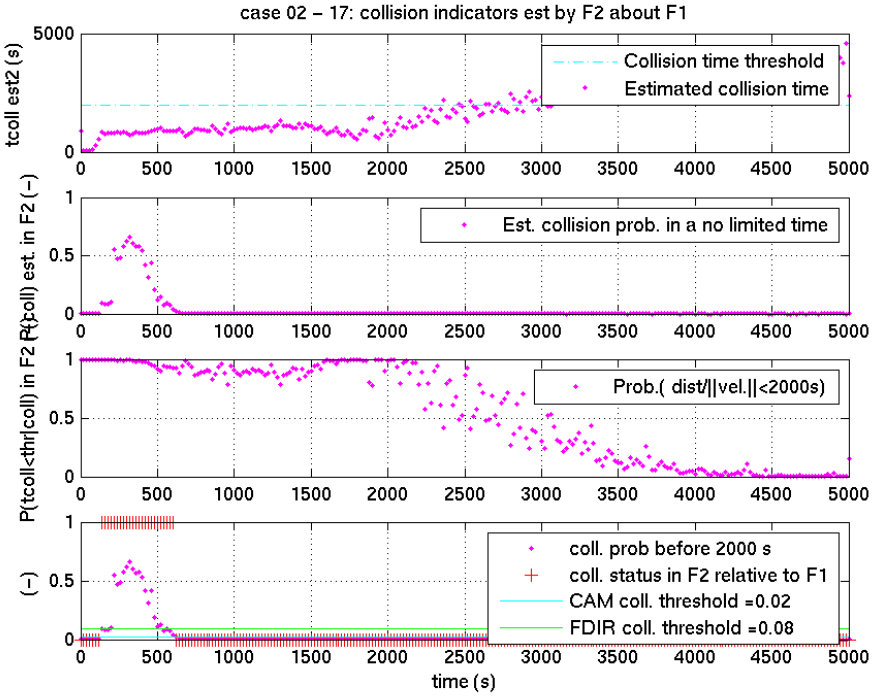

Figure 7-6: Simulation of collision avoidance - a/Time to Go (F1→F2) - b/ collision probability considering direction - c/ collision probability (for time<2000s) considering distance - d/ collision probability= b×c - collision status in CAM

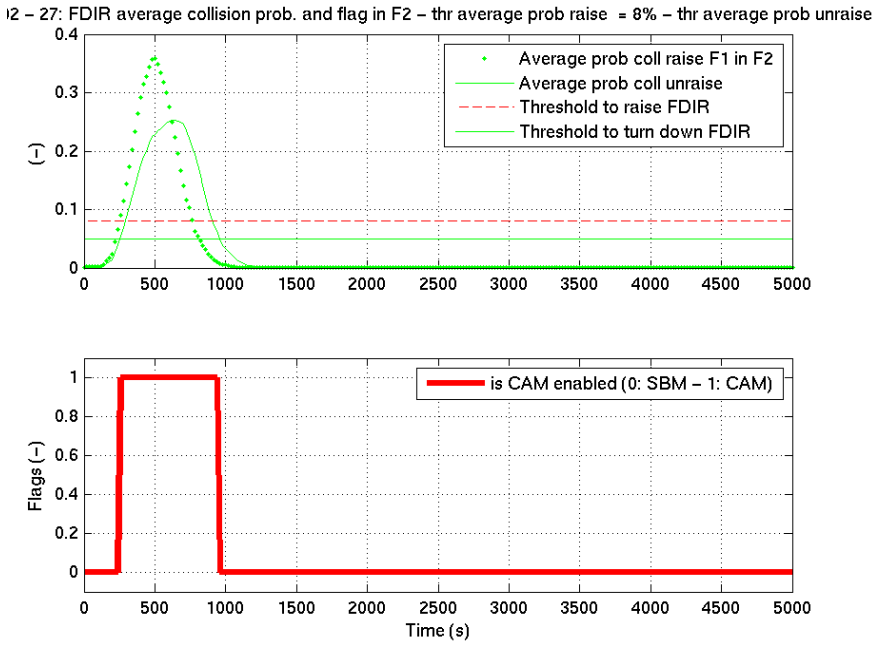

Figure 7-7: Simulation of collision avoidance - FDIR indicator: current mode (0: Stand-By Mode - 1: CAM) - on the 1st chart, the plot with points is the filtered probability which ascending front through the dashed plotted threshold induces a transition to CAM, whereas the plot in solid line is the filtered probability which descending front through the threshold plotted in solid line induces the end of the CAM

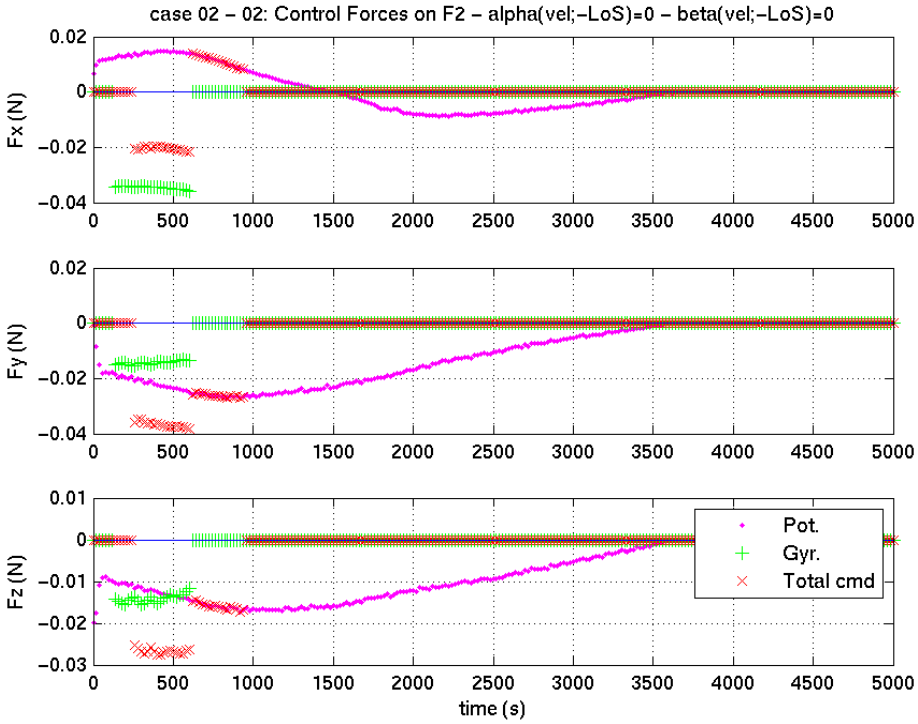

Figure 7-8: Simulation of collision avoidance - Commanded collision avoidance forces on F2

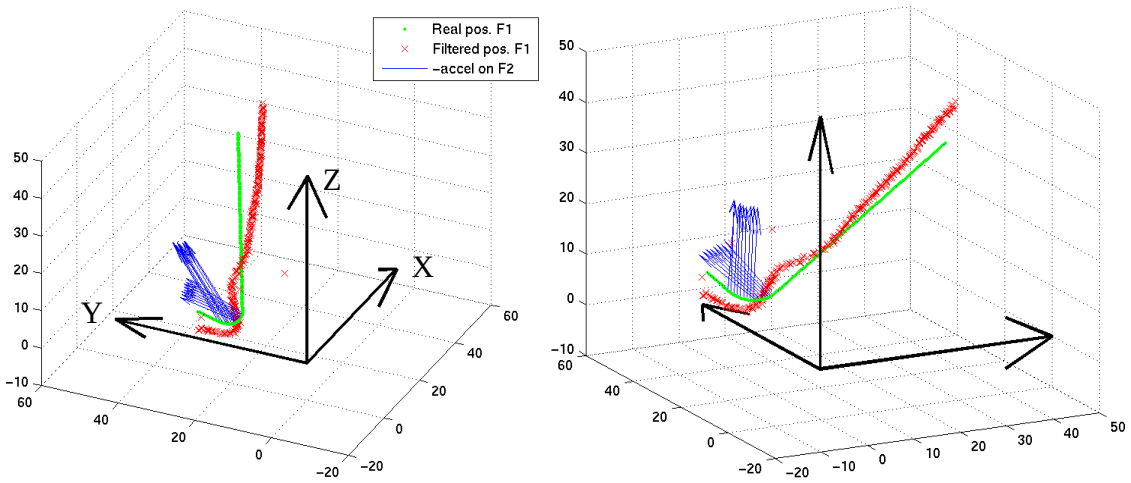

Figure 7-9: Simulation of collision avoidance - Trajectories of F1 and F3 in F2 frame and filtered F1 trajectory - 2 *views*

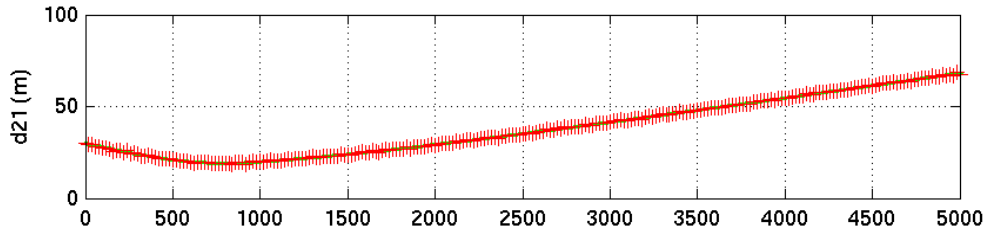

Figure 7-10: Inter-flyers distances (real and estimated)

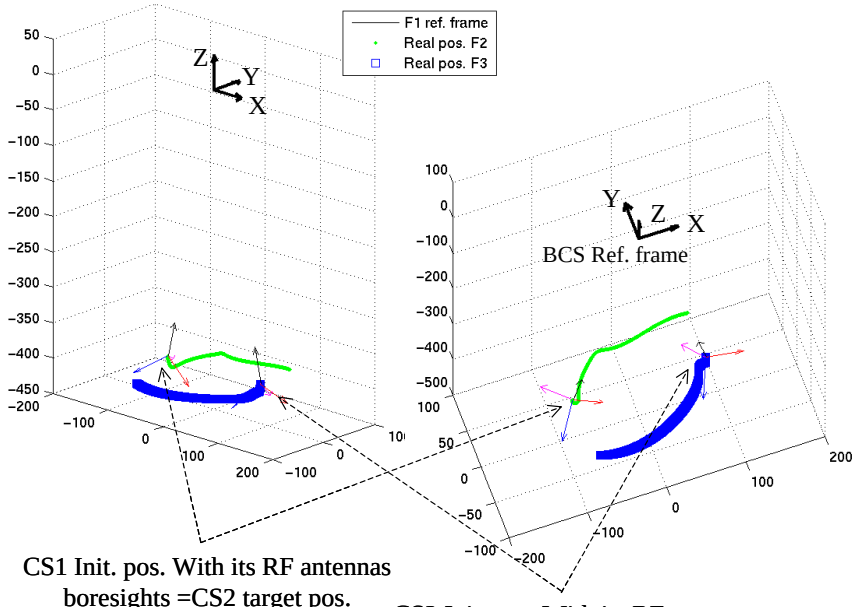

Figure 7-11: Reconfiguration exchanging 2 CS positions w.r.t. BCS with nominal collision avoidance -2 views of the trajectories in BCS frame - RF triplet measurements of CS1 and CS2 are used BIAR - second step AIAR is not simulated

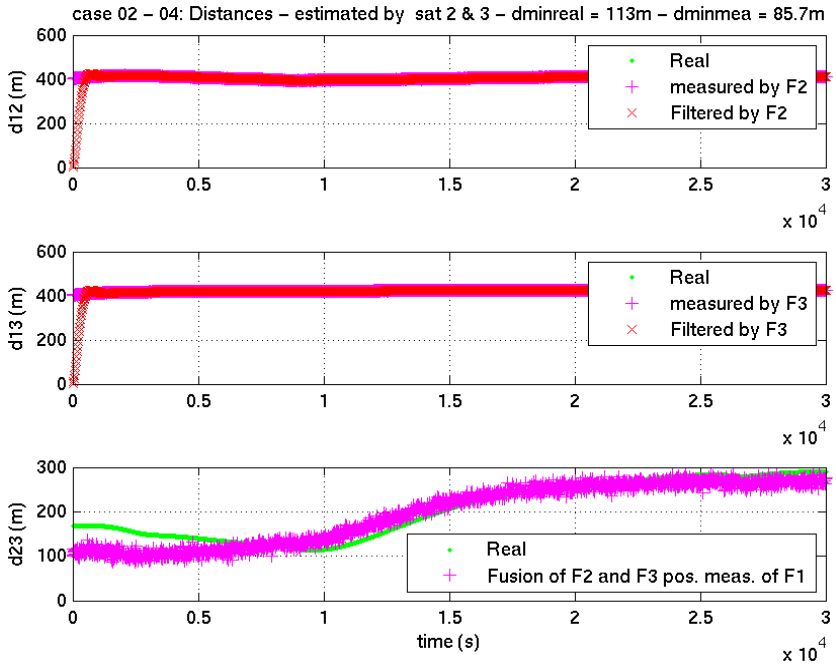

Figure 7-12: Reconfiguration exchanging 2 CS(F2 &F3) positions w.r.t. BCS (F1) with nominal collision avoidance - Real and estimated distances

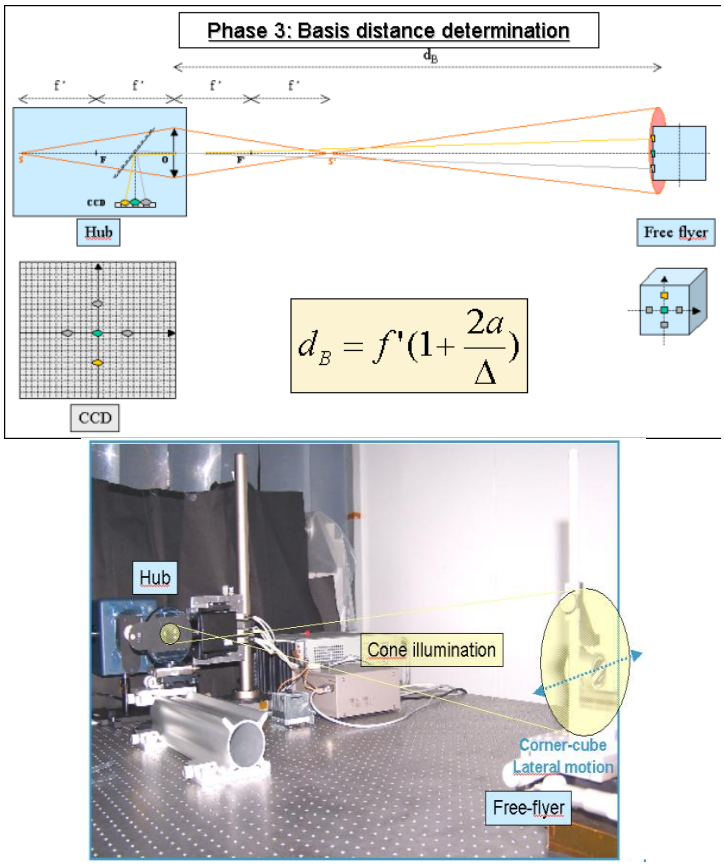

Figure 7-13: ULLIS sensor : principle and breadboard

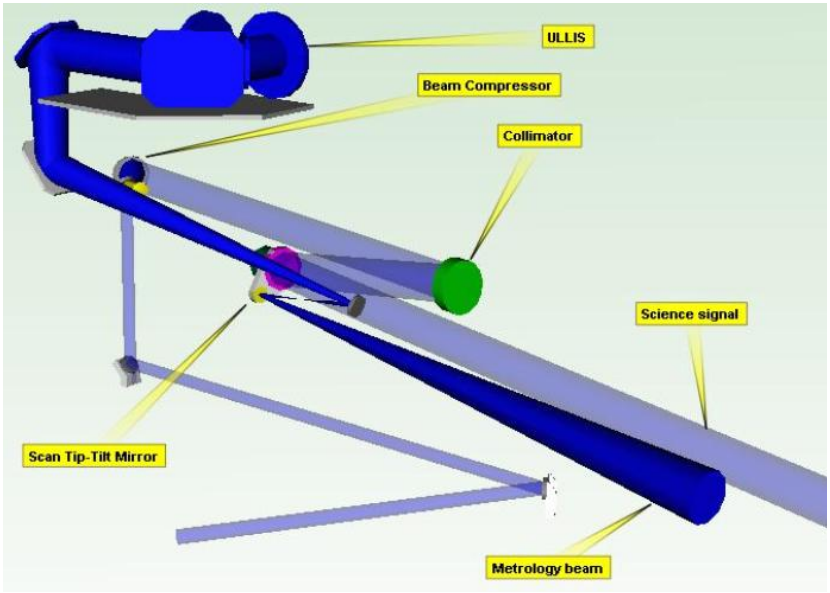

Figure 7-14: A part of the metrology and transfer optics stage on the BCS optical bench : the optical path of one ULLIS metrology beam (dark blue) and of one science beam (light blue). Science beam comes from one collector. The two beams share the same scan tip-tilt mechanisms. They are separated spatially.

Authors

Roland Frenkiel,)Thales Alenia Space, 100 Bd du Midi, BP 99, 06156 Cannes La Bocca Cedex, France.

Contacts: roland.frenkiel@thalesaleniaspace.com.

Laurent Pirson, Thales Alenia Space, 100 Bd du Midi, BP 99, 06156 Cannes La Bocca Cedex, France.

Contacts: laurent.pirson@thalesaleniaspace.com.

Jean-Baptiste Thévenet, Thales Alenia Space, 26 Avenue J.F. Champollion, BP 33787, 31037 Toulouse Cedex 1, France.

Contact : jean-baptiste.thevenet@thalesaleniaspace.com.